Calcified Tissue International (2019) 104:679–689
https://doi.org/10.1007/s00223-019-00528-x

ORIGINAL RESEARCH

Genetic Disruption of *Anoctamin 5* in Mice Replicates Human Gnathodiaphyseal Dysplasia (GDD)

Xiaoyu Wang[1] · Xiu Liu[1] · Rui Dong[1] · Chao Liang[1] · Ernst J. Reichenberger[2] · Ying Hu[1,3]

Received: 11 October 2018 / Accepted: 18 January 2019 / Published online: 2 February 2019

Abstract

Gnathodiaphyseal dysplasia (GDD; OMIM#166260) is a rare skeletal disorder which is mainly characterized by cemento-osseous lesions in mandibles, bone fragility, bowing and diaphyseal sclerosis of tubular bones. GDD is caused by point mutations in *Anoctamin-5* (*ANO5*); however, the disease mechanisms remain unclear. Here we generated *Ano5*-knockout (KO) mice using a CRISPR/Cas 9 approach to study loss of function aspects of GDD mutations. Homozygous *Ano5* knockout mice ($Ano5^{-/-}$) replicate some typical traits of human GDD including massive jawbones, bowing tibia, sclerosis and cortical thickening of femoral and tibial diaphyses. Serum alkaline phosphatase (ALP) levels were elevated in $Ano5^{-/-}$ mice as in GDD patients. Calvaria-derived $Ano5^{-/-}$ osteoblast cultures show increased osteoblastogenesis, which is consistent with our previous in vitro observations. Bone matrix is hypermineralized, and the expression of bone formation-related factors is enhanced in $Ano5^{-/-}$ mice, suggesting that the osteogenic anomaly arises from a genetic disruption of *Ano5*. We believe this new mouse model will shed more light on the development of skeletal abnormalities in GDD on a cellular and molecular level.

Keywords Gnathodiaphyseal dysplasia · Ano5 · Genetic disorder · Skeletal phenotype · Osteoblastogenesis

Introduction

Gnathodiaphyseal dysplasia (GDD; OMIM:16620) is a generalized bone disorder involving cemento-osseous resorptive lesions of the mandible accompanied by a complex skeletal phenotype of bone fragility, cortical thickening and sclerosis of tubular bone diaphyses. Mandibular lesions can lead to recurrent osteomyelitis of the jaw, and the majority of patients suffer from frequent bone fractures as a result of minor accidents or strain. The term "gnathodiaphyseal sclerosis" was first proposed by Akasaka [1] in a large Japanese kindred of 21 patients. Riminucci et al. [2] redefined the terminology to "gnathodiaphyseal dysplasia (GDD)" because osteosclerosis is not found in all patients while some traits of GDD overlap with other syndromes involving fibro-osseous jaw lesions and skeletal dysfunction, most notably fibrous dysplasia (FD) and McCune-Albright syndrome (MAS) [3]. However, the lack of typical radiological changes in bone such as a cotton wool-like pattern in FD and lack of skin pigmentation or endocrinopathies in MAS caused by mutations in GNAS1 differentiates GDD from FD/MAS.

GDD is inherited as an autosomal dominant trait or occurs sporadically and maps to chromosome 11q14.3–15.1 [4]. Eight missense mutations in the *anoctamin 5* (*ANO5; GDD1; TMEM16E*) gene have been identified in families with GDD and in patients with de novo mutations from various races and ethnicities [5–11]. *ANO5* encodes for a 913 amino acid protein and belongs to a family of transmembrane proteins, which in humans includes 10 members. C356R and C356G mutations in ANO5 decreased cell adhesion and changed the cell morphology to a more rounded cell shape, which is possibly due to the regulatory role of ANO5 in intracellular calcium homeostasis [6]. Although

Electronic supplementary material The online version of this article (https://doi.org/10.1007/s00223-019-00528-x) contains supplementary material, which is available to authorized users.

✉ Ying Hu
shuaiyu369@163.com

[1] Beijing Stomatological Hospital, Capital Medical University, Beijing, People's Republic of China

[2] Department of Reconstructive Sciences, Center for Regenerative Medicine and Skeletal Development, University of Connecticut Health, Farmington, CT, USA

[3] Beijing Stomatological Hospital, Beijing Institute of Dental Research, Capital Medical University, No 4 Tiantanxili, Dongcheng District, Beijing 100050, People's Republic of China

some members of this family such as ANO1 and ANO2 act as calcium-activated chloride channels (CaCCs) [12–14], a recent study demonstrated that ANO5 had phospholipid scrambling activity and non-selective ion transport capability [15] and that a T513I mutation [7] in the ANO5 protein caused a gain of function enabling phospholipid scrambling at low cytosolic Ca^{2+} levels. Murine ANO5 is highly expressed in cardiac muscle, skeletal muscle, growth-plate chondrocytes and osteoblasts [16]. Anoctamin 6 (ANO6), another member of the ANO protein family, is involved in hydroxyapatite deposition [17] as well as in control of bone mineralization by activating the calcium transporter NCX1 [18] and as regulator of C2C12 myoblast proliferation [19]. Recessive mutations in the *ANO5* gene cause two types of muscular dystrophies, limb girdle muscular dystrophy type 2L (LGMD2L) and Miyoshi myopathy type 3 (MMD3) [20–22]. While ANO5-related muscular dystrophies have been relatively well researched, the function of ANO5 and the molecular pathophysiology of ANO5 mutations leading to GDD are insufficiently explored.

In our previous study, where we knocked down *Ano5* mRNA in MC3T3-E1 osteoblast precursors we saw elevated expression of osteoblast-related genes such as *Col1a1, osteocalcin, osterix* and *Runx2* as well as increased mineralization during osteoblast differentiation [5]. Several *Ano5* knockout (KO) mouse or rabbit models provide some evidence for reduced capacity to repair sarcolemma, altered lipid metabolism and affecting sperm motility but failed to discuss skeletal phenotypes at all [23–26]. Here we introduce a new *Ano5* knockout mouse model, which replicates clinical features of patients with GDD and exhibits stimulatory effects on osteoblastogenesis.

Materials and Methods

Animals

C57BL/6N mice and Kunming (KM) mice were purchased from Beijing Vital River Laboratory Animal, Co., Ltd. All mice were housed in a specific pathogen-free (SPF) facility. The animal protocol was approved by the Animal Care Committee of Beijing Stomatological Hospital, Capital Medical University, and animal studies were approved by the Institutional Animal Care and Use Committee of the Beijing Stomatological Hospital. Two sgRNAs were designed to target the two sides of exons 11–12 (Fig. 1a). For each targeting site, candidate guide RNAs were designed by the CRISPR design tool (http://crispr.mit.edu). Guide RNAs were screened for on-target activity using the Universal CRISPR Activity Assay (UCATM).. C57BL/6 female mice and KM mouse strains were used as embryo donors

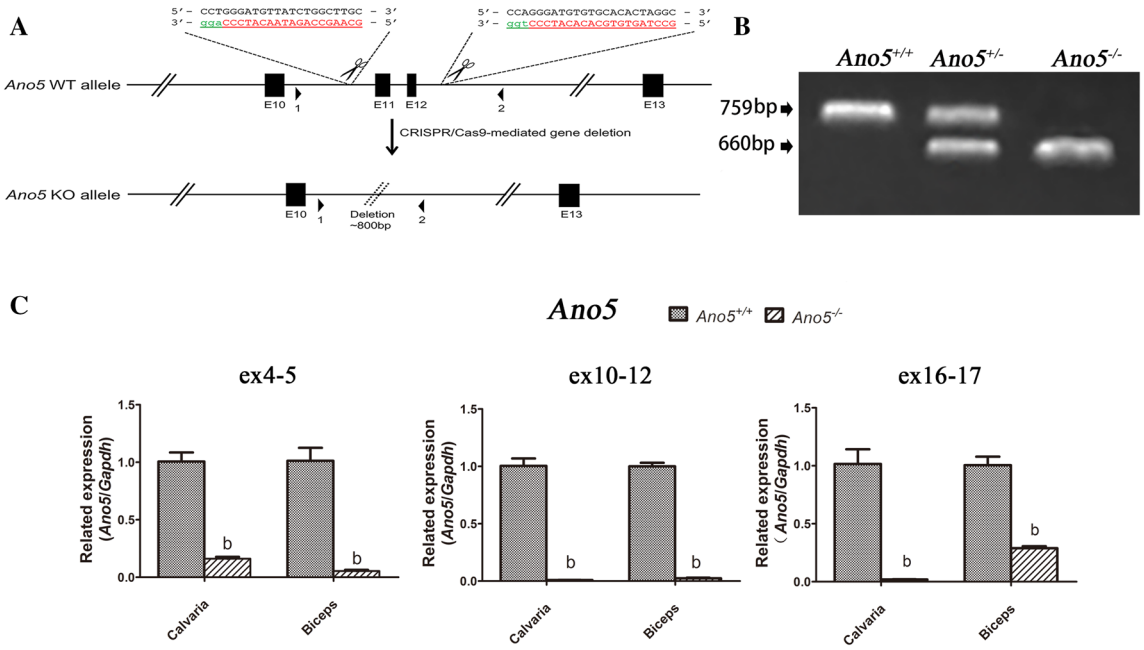

Fig. 1 Generation and genotyping of $Ano5^{-/-}$ mice. (**A**) Schematic overview of strategy to generate *Ano5* KO allele. The guide RNA sequence is underlined, capitalized, and labeled in red. The protospacer-adjacent motif (PAM) sequence is labeled in green. The arrowheads indicate locations of primers 1 and 2 used for PCR. (**B**) PCR genotyping assay for $Ano5^{+/+}$, $Ano5^{+/-}$, and $Ano5^{-/-}$mice. Wild type allele: 759 bp, mutant allele: 660 bp. (**C**) Approximately 80% and >99% relative reduction of *Ano5* transcript, at the 5' and 3' end, respectively, was confirmed by qRT–PCR in in different mouse tissues extracted from the $Ano5^{-/-}$ mouse. Five mice of each group were used; $^{b}P < 0.01$ indicates statistical significance by one-way ANOVA

and pseudopregnant foster mothers, respectively. Genomic DNA was extracted from mouse tails using an alkaline lysis method. PCR genotyping generates a 759-bp product for wild type and a 660-bp product for mutant *Ano5* (Fig. 1b). Mice were backcrossed with C57BL/6N mice and bred for at least four generations to demonstrate hereditary stability.

Skeletal Imaging Analysis

Mandibles, femurs and tibias of 12-week-old $Ano5^{+/+}$ male mice ($n=8$) and their $Ano5^{-/-}$ littermates ($n=9$) were used for X-ray and Micro Computed Tomography (μCT) analysis. This age is equivalent to adulthood in humans, when most of the GDD patients display symptoms. Radiographs of individual bones were taken using a MX20 Radiography System (Faxitron X-ray) with exposure of 0.125 s. μCT was performed with 14 μm resolution in the Central Laboratory of the Capital Medical University (CCMU) (Inveon CT, Siemens, Germany). Mandibular images were obtained by capturing vertical sections at the central fossa of mandibular first molars. For CT scanning, cancellous mandibular bone surrounding the first molar was chosen as the area of interest in $Ano5^{+/+}$ and $Ano5^{-/-}$ groups. Trabecular measurements of tubular bones were taken at the distal growth plate in 70 consecutive 14 μm slices over a distance of 980 μm. Thirty cross sections in the mid-diaphysis were used to compute cortical bone parameters. Hounsfield unit (HU) and calibrated CT data were applied to calculate bone mineral density (BMD) according to phantom reference data. Bone volume was calculated by an interactive medical image control system (Mimics19.0, Materialise, Belgium) combined with BMD to acquire bone mineral content (BMC).

Mouse Serum Analysis

Serum was prepared from retro-orbital blood sampling of 12-week-old male mice after 1-h incubation at 4 °C and 5 min centrifugation at 3000 rpm. Serum TRACP 5b (Tartrate-Resistant Acid Phosphatase-5b ELISA Kit, MyBioSource, USA) was detected in $Ano5^{+/+}$, $Ano5^{+/-}$ and $Ano5^{-/-}$ mice. Alkaline phosphatase (ALP) activity was determined according to manufacturer's specification (Nanjing Jiancheng, China). The number of samples used for serum analysis was a minimum of 7 per group ($n \geq 7$).

Bone Tissue Morphology

Mandibles, tibias and femurs of 12-week-old male mice were fixed for 48 h in 4% PFA and then decalcified in 10% EDTA solution and processed for paraffin embedding. Series of 5-μm-thick longitudinal and horizontal sections were cut from paraffin sections of the $Ano5^{+/+}$, $Ano5^{-/-}$ groups ($n \geq 5$) stained with hematoxylin-eosin (H&E). For immunohistochemical (IHC) staining, antigens in paraffin-embedded mandible samples were retrieved by 0.01 M citric acid buffer (pH 6.0). Endogenous peroxide activity was quenched with 3% hydrogen peroxide. Slides were incubated in blocking solution with 10% goat serum for 15 min prior to overnight incubation at 4 °C with primary antibodies against CD31 (Abcam, ab28364,1:200, UK), TNF-α (Abcam, ab6671, 1:500, UK) and IL-6 (Abcam, ab7737, 1:500, UK), respectively. Slides were incubated with a biotin-labeled secondary goat anti-rabbit IgG antibody (ZSGB-BIO, SP-9001, China) for 30 min at 37 °C, visualized with diaminobenzidine and counterstained with hematoxylin. Slides were imaged with an Olympus BX61 microscope (Olympus, Japan), and immuno-positive areas were analyzed by Image-Pro Plus 6.0 (Media cybernetics, USA).

Mouse Calvarial Osteoblast Cultures (mCOBs)

Calvariae from postnatal 24-h-old littermates were isolated and digested with 0.3% collagenase (Type I; Sigma-Aldrich, USA) mixed with equal volume 0.05% trypsin (Invitrogen-Gibco, USA). Calvariae were digested for four cycles at 15 min/cycle at 37 °C. Cells of the first cycle were discarded, and the remaining cells were collected and cultured in DMEM (Gibco, USA). Medium was switched to osteoblast differentiating medium (α-MEM; Invitrogen-Gibco, USA) containing 10% fetal bovine serum (FBS; Gibco, USA), 1% dual-antibiotics (Gibco, USA), 4 μg/ml dexamethasone, 50 mg/ml ascorbic acid and 4 mM β-glycerophosphate (Sigma-Aldrich, USA) for osteoblast differentiation. Cells were derived from no less than five mice in each group. Medium was changed three times a week.

Matrix and Mineralization Assays

Alizarin red staining and alkaline phosphatase activity detection were performed to observe the formation of matrix and mineralization. Osteoblasts (passage 2) were seeded at a density of 2×10^5 cells per well in 6-well plates. Alizarin red staining was performed at 7, 14 and 21 days of culture, and mineralized nodules were dissolved by cetylpyridinium chloride for 30 min. Calcium binding to alizarin red was detected by colorimetric detection as indicator for calcification. Absorbance reads were determined at 562 nm. Protein for ALP analysis was extracted and quantified by BCA to assess early osteogenic differentiation at 0, 3, 5 and 7 days. ALP activity was detected by an Alkaline Phosphatase Assay Kit (Nanjing Jiancheng, China) according to manufacturer's instructions. OD values were measured at 520 nm.

RNA Analysis

We used quantitative real-time PCR (qRT-PCR) to detect expression of *Ano5* and osteogenic factors in bone tissue and mCOBs, respectively. PCR primers are listed in Supplementary Table 1. Total RNA derived from tissues or primary cultured cells was extracted with TRIzol (Invitrogen, USA) followed by reverse transcription (SuperRT cDNA Synthesis Kit; CWbio, China). qRT-PCR was carried out using Ultra SYBR Mixture with low ROX (CWbio, China) in a Bio-Rad thermocycler (BioRad, Hercules, USA). Relative quantification of gene expression was measured by the ΔΔCt method and the housekeeping gene *Gapdh* served as control.

Statistical Analysis

Statistical analysis was performed by paired t test or one-way ANOVA using Prism7 software (GraphPad Software, La Jolla, USA).

Results

Generation and Appearance of *Ano5*$^{-/-}$ Mice

We targeted exons 11 and 12 to produce a truncated transcript with a 833 bp deletion. To investigate the expression of *Ano5* transcripts, we performed qRT-PCR with primers spanning exons 4–5, 10–12 and 16–17. In *Ano5*$^{-/-}$ mice, expression of *Ano5* in skull and musculus biceps brachii dropped to almost zero (background level) when the primers span exons 10–12, suggesting complete knockout of *Ano5*. qRT-PCR with primers span exons 4–5 or exons 16–17 shows ~ 80% reduction of pre-deletion *Ano5* transcripts in all tissues tested and > 99% reduction of post-deletion *Ano5* transcript in calvariae and > 71% reduction of post-deletion *Ano5* transcript in muscle (Fig. 1c). Behavior and overall appearance of *Ano5*$^{-/-}$ mice was comparable to normal littermates, and *Ano5*$^{-/-}$ male mice showed low fertility compared with heterozygotes and wild type mice (data not shown).

GDD-Like Skeletal Phenotype of Ano5$^{-/-}$ Mice

GDD is clinically diagnosed by histological analysis of bone lesions in the jaws combined with radiography [3, 8]. We performed radiography on mandibles, femurs and tibias of 12-week-old male littermates in more than 10 animals per group. Similar to GDD patients, *Ano5*$^{-/-}$ mice showed increased radiopacity of mandibles and cortical bone of femurs and tibiae. Mandibles of 12-week-old *Ano5*$^{-/-}$ mice were larger with increased bone density (Fig. 2a). Femoral length or width was not significantly different. To better illustrate the skeletal phenotype, we studied the bones by μCT. *Ano5*$^{-/-}$ mice had increased BMC and BMD in mandibles and in diaphyses of cortical bones (Table 1). Mandibles of *Ano5*$^{-/-}$ mice displayed hyperostosis (Fig. 2b), which is consistent with our X-ray results, whereas the bone volume fraction (BVF) in tibiae and femurs was reduced. Two notable characteristics of GDD patients are bowing of tibia, and bone fragility combined with cortical thickening of diaphyses. *Ano5*$^{-/-}$ mice exhibited abnormal shape of tibiae with increased diameter of diaphyseal cortices for both tibiae and femurs resulting in narrow medullary canals (Fig. 2c, d). The mandibles and diaphyses of femurs and tibiae were undertrabeculated in *Ano5*$^{-/-}$ mice with significantly reduced thickness and trabecular numbers compared to *Ano5*$^{+/+}$ mice. The trabeculation of *Ano5*$^{-/-}$ mice was more significantly dispersed in mandibles and femoral diaphyses but normal in tibia (Table 2). In addition, heterozygous *Ano5*$^{+/-}$ mice were phenotypically similar to *Ano5*$^{-/-}$ mice and exhibited measurable GDD-like skeletal phenotypes as they aged.

Biochemical Analysis of Ano5$^{-/-}$ Mice

Serum alkaline phosphatase levels are variable but generally elevated in GDD patients [2, 8, 11]. Therefore, we tested the ALP activity of 12-week-old *Ano5*$^{-/-}$ mice and found that ALP in sera of *Ano5*$^{-/-}$ and *Ano5*$^{+/-}$ mice was increased by approximately 23% (Fig. 3a). To investigate the activity of osteoclasts, we measured the levels of TRACP 5b. Previously only one GDD patient was reported with elevated TRACP near the upper normal limits [27]. In the mouse model, we found comparable TRACP values in *Ano5*$^{-/-}$, *Ano5*$^{+/-}$ and *Ano5*$^{+/+}$ mice (Fig. 3b).

Morphological Analysis of Bone Tissues in Ano5$^{-/-}$ Mice

Histological sections stained with H&E confirmed that *Ano5*$^{-/-}$ mice had thicker cortical bones in cross sections of mandibles (Fig. 4a). Being consistent with the results from μCT, *Ano5*$^{-/-}$ mouse tibia exhibited cortical thickening and bowing. Tibial bowing is quite variable in *Ano5*$^{-/-}$ mice, as can be seen in Figs. 2a and 4b. Moreover, trabeculation is decreased drastically outside the metaphyseal region of femurs or tibiae of *Ano5*$^{-/-}$ mice (Fig. 4b). *Ano5*$^{-/-}$ mice have approximately threefold more blood vessels in the periodontal ligament of first molars than *Ano5*$^{+/+}$ mice based on CD31 expression (Fig. 4c), and this may indicate beginning periodontal ligament hyperemia. Meanwhile, expression of TNF-α and IL-6 in blood vessels of the periodontal ligament of *Ano5*$^{-/-}$ mice was increased dramatically ($P < 0.01$ for TNF-α and IL-6), which suggest that *Ano5*$^{-/-}$ mice may suffer from periodontal inflammation (Fig. 4d).

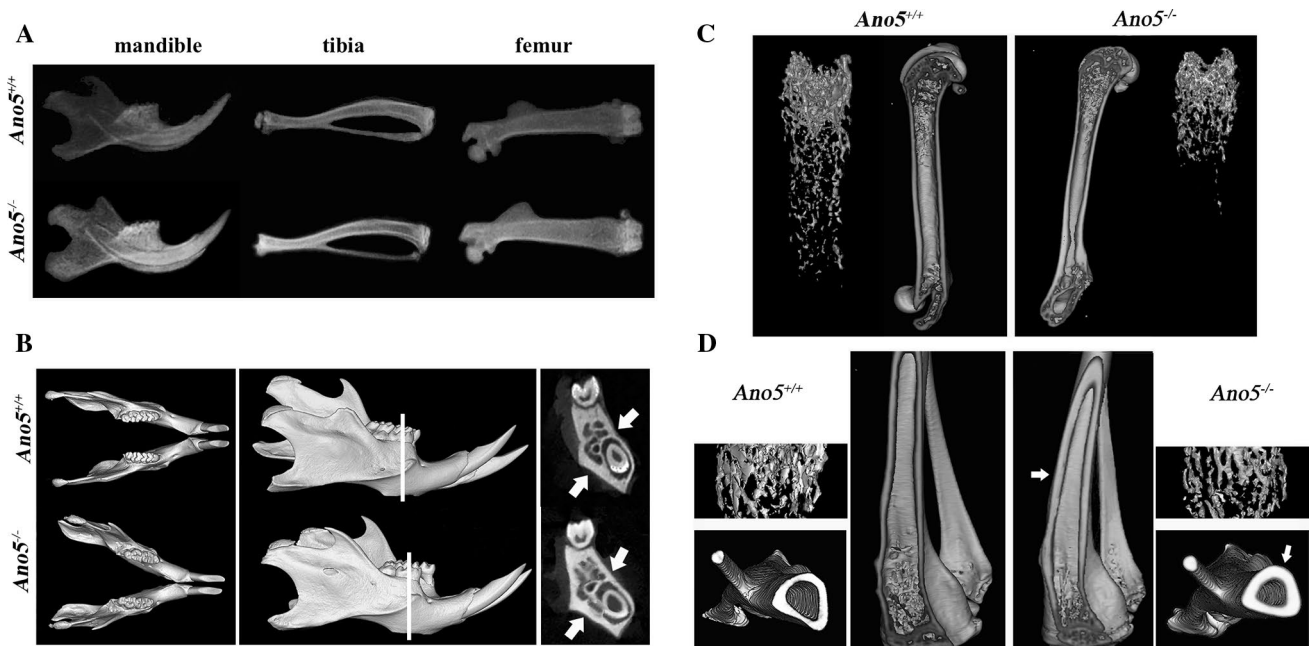

Fig. 2 GDD-like phenotype in 12-week-old *Ano5*$^{-/-}$ mice. (**A**) Representative radiographs of mandibles, tibias and femurs from 12-week-old *Ano5*$^{+/+}$, *Ano5*$^{+/-}$, and *Ano5*$^{-/-}$ male mice. (**B**) μCT images of vertical plane through mandibles and 3D reconstruction of mandibles from *Ano5*$^{+/+}$ and *Ano5*$^{-/-}$ mice. White line points to sagittal plane through central fossa of first mandibular molar. White arrows points to the hyperostosis of mandibles. (**C**) Internal view of femurs in longitudinal section and 3D reconstructions of trabeculae in diaphysis from *Ano5*$^{+/+}$ and *Ano5*$^{-/-}$ mice. (**D**) Internal view in longitudinal section and cross-section of cortical bone of tibia. 3D reconstructions of trabeculae in metaphysis of *Ano5*$^{+/+}$ and *Ano5*$^{-/-}$ mice

Table 1 BMC and BMD analysis of *Ano5*$^{+/+}$ and *Ano5*$^{-/-}$ male mice

	Ano5$^{+/+}$ ($n=8$)			*Ano5*$^{-/-}$ ($n=9$)		
	Mandible	Tibia	Femur	Mandible	Tibia	Femur
BMC (g)	0.040 ± 0.005	0.062 ± 0.001	0.090 ± 0.003	0.051 ± 0.004**	0.071 ± 0.003**	0.098 ± 0.002**
BMD (g/cc)	2.834 ± 0.031	2.805 ± 0.038	2.800 ± 0.012	2.967 ± 0.071*	2.911 ± 0.035*	2.901 ± 0.030**

Measurements of mice at 12 wk of age were taken by μCT. Data are mean ± SD for groups of 8–9 mice. *$P<0.05$, **$P<0.01$

Bone Matrix and Mineral Formation

In consideration of the high expression of ANO5 protein in osteoblasts and evidence from our previous study suggesting a potential role of ANO5 in osteoblastogenesis [4], we determined the mineralization potential of cultured mCOBs by alizarin red staining. Osteoblast cultures from *Ano5*$^{-/-}$ mice developed more mineral nodule deposition over a 21-day culture period in osteogenic medium (Fig. 5a, b). Quantitative analysis also showed that the Ca^{2+} concentration was elevated in the *Ano5*$^{-/-}$ group after nodule dissolution (Fig. 5c). *Ano5*$^{+/-}$ mice showed intermediate levels of mineralization compared to *Ano5*$^{+/+}$ and *Ano5*$^{-/-}$ mice. The highest ALP activity in osteoblasts occurred at culture day 5 and decreased by day 7 in both groups (Fig. 5d). However, *Ano5*$^{-/-}$ mice showed significantly higher ALP activity than *Ano5*$^{+/+}$ mice at all time points ($P<0.01$). Increased mineralization and ALP activity in *Ano5*$^{-/-}$ osteoblast cultures are consistent with our previous *in vitro* finding, where the overexpression of a GDD mutation resulted in increased mineralization [5].

Osteogenesis-Related Factors Increase in Ano5$^{-/-}$ Mice

To investigate whether deficit of *Ano5* affects expression of osteoblast differentiation markers, we performed qRT-PCR of mRNA isolated from 0-, 3-, 7-, 14- and 21-day mCOB cultures of *Ano5*$^{+/+}$, *Ano5*$^{+/-}$ and *Ano5*$^{-/-}$ mice in osteogenic medium. We found that expression of *collagen I* (*Col1a1*) and *Bglap* (*osteocalcin, Ocn*) in mCOBs gradually increased in *Ano5*$^{+/+}$, *Ano5*$^{+/-}$ and *Ano5*$^{-/-}$ mice over time (Fig. 6a, b). *Spp1* (*osteopontin, Opn*), *Runx2, Sp7* (*osterix*) and *Tnfrsf11b* (*osteoprotegerin, Opg*) showed higher expression at day 7

Table 2 μCT analysis of *Ano5*+/+ and *Ano5*-/- male mice

	Ano5+/+ ($n=8$)	*Ano5*-/- ($n=9$)
Mandibles		
Dentin density	1136.33 ± 32.31	1364.48 ± 38.50*
BV/TV(%)	70.44 ± 1.80	65.62 ± 1.53*
Bone surface/bone vol (1/mm)	22.02 ± 0.58	25.02 ± 0.11*
Trabecular thickness (μm)	83.04 ± 2.26	77.37 ± 1.74*
Trabecular number	8.50 ± 0.11	7.68 ± 0.16*
Trabecular spacing (μm)	36.78 ± 3.81	42.94 ± 3.64**
Trabecular pattern factor	0.62 ± 0.14	2.68 ± 0.39*
Femurs		
BV/TV(%)	35.57 ± 1.60	10.41 ± 2.03**
Bone surface/bone vol (1/mm)	38.75 ± 1.70	50.15 ± 1.05**
Trabecular thickness (μm)	52.15 ± 1.56	39.90 ± 0.85**
Trabecular number	4.68 ± 0.49	2.60 ± 0.44**
Trabecular spacing (μm)	146.73 ± 7.43	355.79 ± 67.72**
Trabecular pattern factor	9.70 ± 1.15	18.81 ± 1.18**
Cortical wall thickness (μm)	236.67 ± 16.99	320.00 ± 21.60*
Tibias		
BV/TV(%)	39.23 ± 0.6	27.99 ± 2.0**
Bone surface/bone vol (1/mm)	33.45 ± 1.69	40.23 ± 1.04*
Trabecular thickness (μm)	60.26 ± 3.14	46.80 ± 4.65*
Trabecular number	6.62 ± 0.29	5.58 ± 0.43*
Trabecular spacing (μm)	101.92 ± 11.67	116.07 ± 6.32
Trabecular pattern factor	3.08 ± 0.54	8.86 ± 1.79*
Cortical wall thickness (μm)	206.67 ± 17.0	303.33 ± 17.0**

Data of 12-week-old male mice were measured by μCT

Data are mean ± SD

BV bone volume, *TV* total volume

*$P<0.05$, **$P<0.01$

with a peak at day 14 in mCOBs from $Ano5^{-/-}$ mice compared to $Ano5^{+/+}$ mice (Fig. 6c–f). Interestingly, the ratio of *Opg* and *Tnfsf11* (*NF-kB ligand, Rankl*) in $Ano5^{-/-}$ mouse osteoblasts significantly increased at days 7 and 14 compared to $Ano5^{+/+}$ osteoblast cultures but was comparable at day 21 (Fig. 6h). This may be due to the high expression of *Rankl* at day 21 (Fig. 6g). It was recently reported that another member of the anoctamin family, *ANO6*, is involved in the control of bone mineralization [17, 18]. We found the expression of *Ano6* elevated in $Ano5^{+/-}$ and $Ano5^{-/-}$ mCOBs at the time of osteoblast extraction and was lower starting at day 3 when compared $Ano5^{+/+}$ cultures (Fig. 6i).

Discussion

The *ANO5* gene is abundantly expressed in skeletal and cardiac muscle as well as in chondrocytes and osteoblasts [16]. This suggests that ANO5 protein plays an essential role in muscle and bone development. Disruption of *ANO5* is associated with autosomal dominant GDD and two autosomal recessive muscular dystrophies, limb girdle muscular dystrophy type2 (LGMD2L) and Miyoshi muscular dystrophy 3 (MMD3) [28–32]. Biochemical properties and physiological function of ANO5 are incompletely understood, and skeletal phenotypes in existing mouse models have not been investigated. We generated an *Ano5* knockout mouse model to study the effect of reduced expression of ANO5 on bone development. We investigated $Ano5^{+/+}$ and $Ano5^{-/-}$ mice as well as $Ano5^{+/-}$ mice at 12 weeks, which exhibit an intermediate phenotype. It will be interesting to follow the progression of their GDD-like phenotype to an older age. GDD in humans is an autosomal dominant disorder. However, it is not uncommon that the phenotypes of a dominant disorder are best replicated in homozygous mutant mouse models [33–36]. This discrepancy may be due to species-specific phenotypic thresholds and lifespan [33, 34]. $Ano5^{-/-}$ mice exhibit distinct features of GDD including elevated ALP levels in serum, mandibles with increased radiopacity, bowing and thicker cortical bone in long bones, which is also found in some clinical GDD reports [1, 2, 5, 8]. However, some mandibular phenotypes such as osteomyelitis, cemento-ossifying fibroma and cementum-like materials were not found in $Ano5^{-/-}$ mice at the age of 3 months. Some pathological

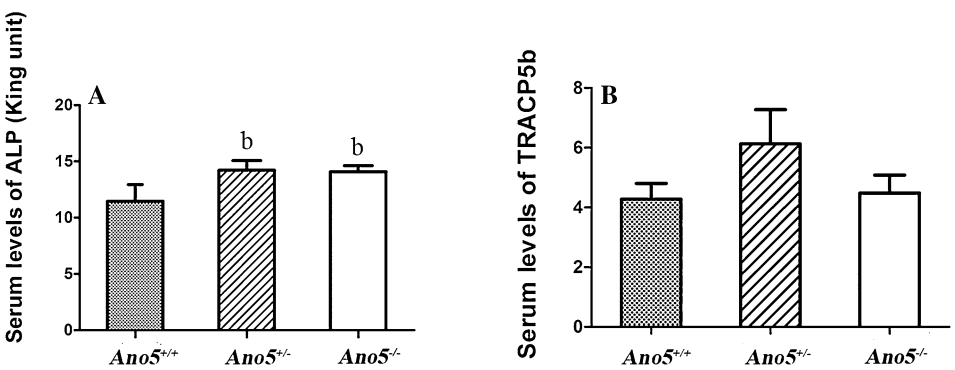

Fig. 3 Serum alkaline phosphatase (ALP) analysis and matrix and mineral formation in mouse calvarial osteoblast (mCOB) cultures. (**A**) Elevated serum ALP was detected in 12-week-old $Ano5^{+/-}$ and $Ano5^{-/-}$ mice but no significant changes of TRACP5b (**B**) compared to $Ano5^{+/-}$ male mice ($n \geq 7$). $^{b}P<0.01$

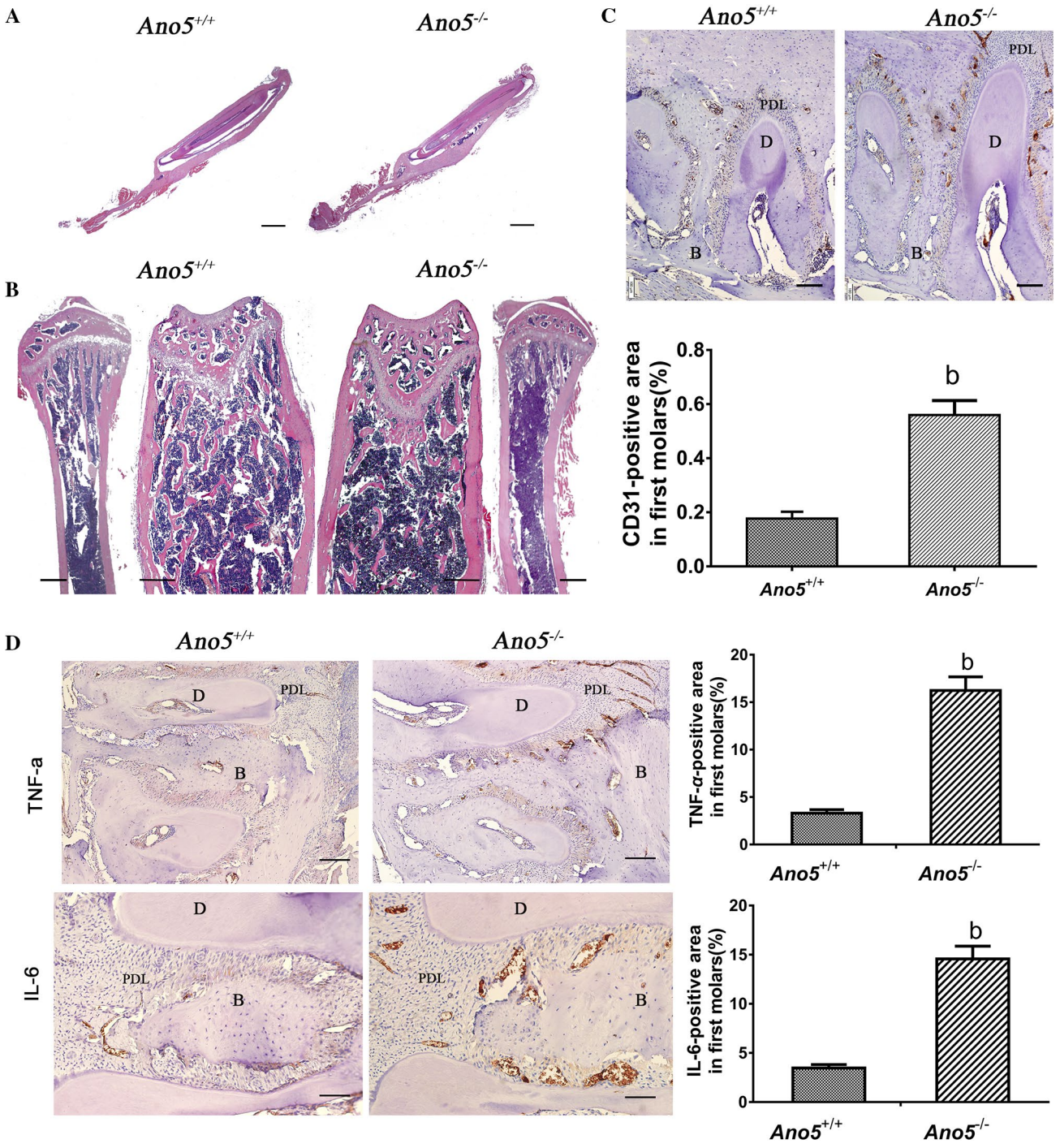

Fig. 4 Histology of *Ano5*$^{+/+}$ and *Ano5*$^{-/-}$ male mice. (**A**) Mandible in vertical plane of from 12-week-old mice (H&E). (**B**) H&E staining of tibias and femurs of 12-week-old mice: tibias, scale bar = 1 mm; femurs, scale bar = 200 µm. (**C**) Representative image showing increased angiogenesis at first molars of *Ano5*$^{-/-}$ mice stained by CD31 and quantified area of blood vessels shown in bar graph below. D, dentin; B, alveolar bone; PDL, periodontal ligament. Scale bar = 100 µm. $^{b}P < 0.01$. (**D**) Representative photomicrographs and quantitative immunopositive areas analysis of TNF-α and IL-6 staining in periodontal ligament of the first molars in *Ano5*$^{+/+}$ and *Ano5*$^{-/-}$ mice. D, dentin; B, alveolar bone; PDL, periodontal ligament. TNF-α, scale bar = 100 µm; IL-6, scale bar = 50 µm. $^{b}P < 0.01$

features may require longer time to develop or may develop only after challenging the mouse. It is also possible that some additional factors that trigger manifestation of certain aspects of the disorder are different in mice and humans, such as the immune system, metabolism or other biological characteristics [37, 38]. Interestingly, we found increased

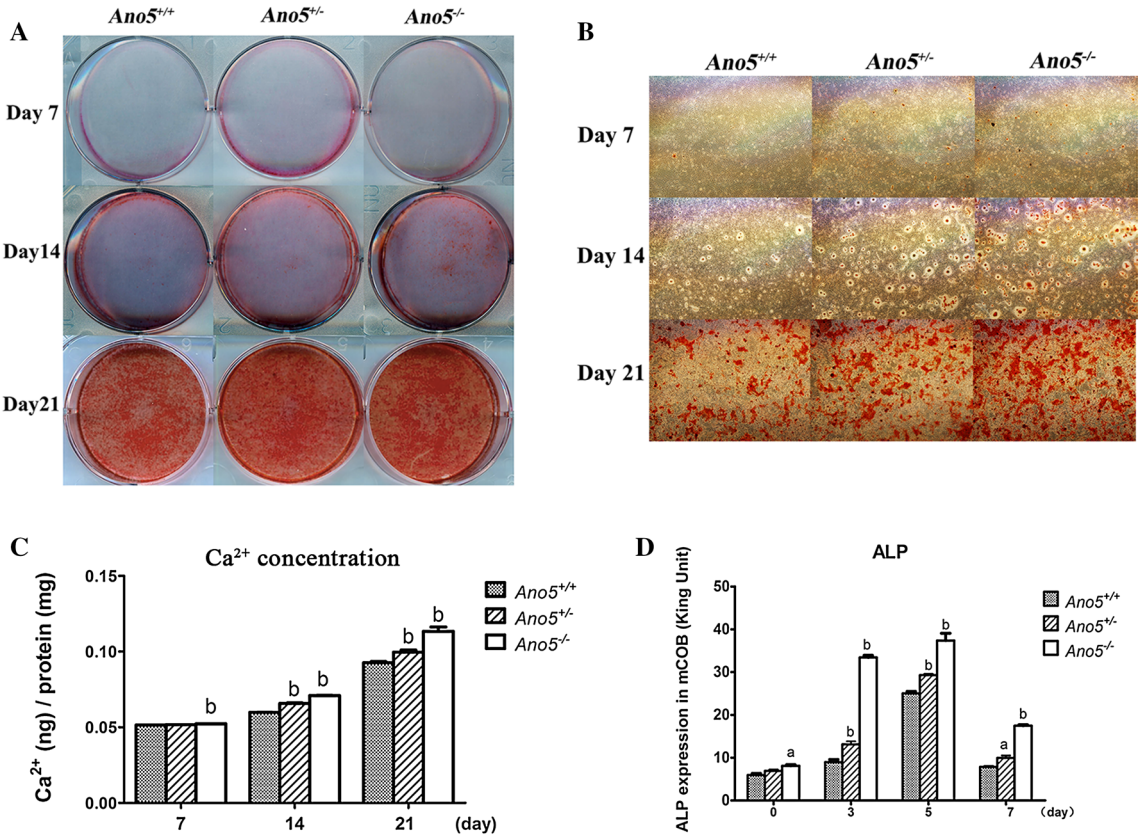

Fig. 5 Mineralization of mouse calvarial osteoblast cultures. (**A**) General observation and (**B**) microscopic observation of *Ano5*$^{+/+}$ and *Ano5*$^{-/-}$ mCOBs stained for alizarin red S at culture days 7, 14 and 21. (**C**) Histogram representing corresponding calcium binding levels. (**D**) ALP detected in *Ano5*$^{+/+}$ and *Ano5*$^{-/-}$ mCOBs at days 3, 5 and 7. $^{a}P<0.05$, $^{b}P<0.01$

blood vessel formation in the periodontal ligament (PDL) of *Ano5*$^{-/-}$ mice, which suggests a hyperemic state in the early stage of inflammation and therefore we considered the possibility that the mice are in the process of developing inflammatory signs of periodontitis. This speculation was confirmed by evidence of enhanced TNF-α and IL-6 expression in periodontal ligaments of *Ano5*$^{-/-}$ mice. Coincidentally, some adult patients with GDD suffer from painful swelling and purulent discharge from gingiva, loosening or displaced teeth and insufficient healing after tooth extraction [7, 20]. We also have to consider that knockout mice exhibit only those phenotypes that are due to loss of ANO5 function.

Besides increased cytokine expression in the jawbones, *Ano5*$^{-/-}$ mice display thickening of cortical diaphyses and trabecular abnormalities in tubular bones based on our μCT and histomorphometry findings. Decreased trabecular thickness and trabecular number suggest reduced bone remodeling activity that result in sparser trabecular bone with poor connectivity. These changes suggest that *Ano5*$^{-/-}$ mice may be more vulnerable to bone injury. Reduced cancellous bone plays a predominant role for susceptibility to osteoporotic fractures for GDD patients. Increased BMD and BMC in mandibles, femurs and tibiae of *Ano5*$^{-/-}$ mice are consistent with sclerosis and increased diameters of cortical bone found by histology. A recent study in a 13-year-old GDD patient showed that BMD in the radius increased by 20% within a year [8]. Overall bone strength is determined by structural and material components. Therefore, it is possible that cortical thickening in diaphyses is an attempt to compensate for poor bone quality induced by abnormal distribution of trabecular bone in *Ano5*$^{-/-}$ mice. However, over-ossification may inversely increase bone fragility.

Total serum ALP is widely used to assess bone metabolism. Three GDD patients have been reported with elevated levels of serum ALP [2, 8, 11]. While we found increased ALP in serum and in cultured calvarial osteoblasts from *Ano5*$^{-/-}$ mice, the serum TRACP5b level was comparable between *Ano5*$^{+/+}$ and *Ano5*$^{-/-}$ mice. Therefore, we speculate that *Ano5* deficiency may contribute to changes in osteoblastogenesis. Mineralization markers were increased in *Ano5*$^{-/-}$ mice during osteoblastic differentiation. Osteocalcin and *Col1a1*, which are associated with increased mineral deposition, are highly expressed at day 21 of *Ano5*$^{-/-}$ mCOB

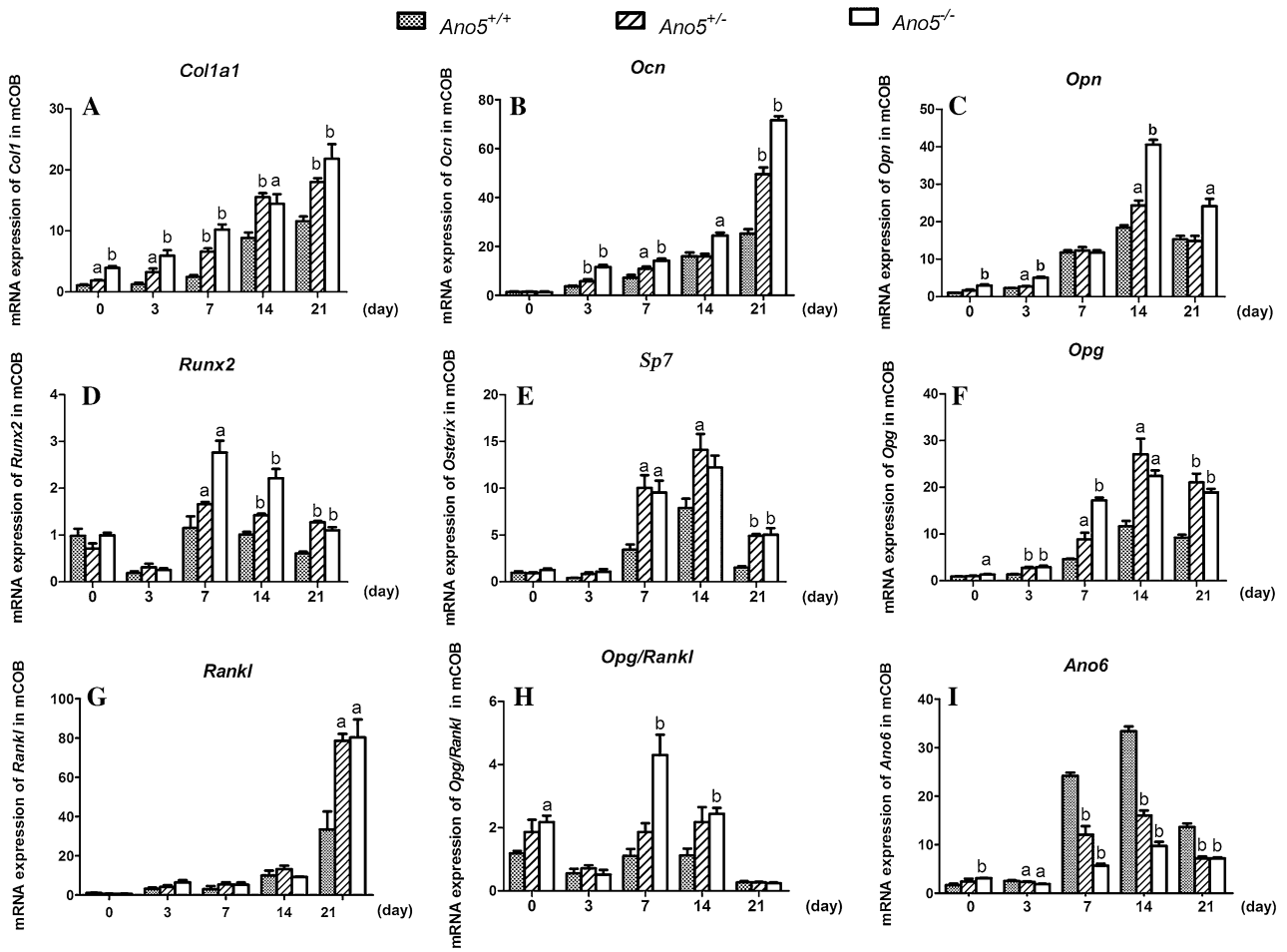

Fig. 6 Osteogenesis-related gene expression in mCOBs from *Ano5*$^{+/+}$ and *Ano5*$^{-/-}$ mice. qPCR analysis of Col1α1, Ocn, Runx2, SP7, Opn, Opg, Rankl, Opg/Rankl and Ano6 at days 0, 3, 7, 14 and 21 *Ano5*$^{-/-}$ calvarial osteoblast cultures normalized to expression levels of *Ano5*$^{+/+}$ cells. Data from three independent experiments. $^{a}P<0.05$, $^{b}P<0.01$

cultures [31]. This may be a result of increased expression of *Runx2* and *SP7*, which are required for osteoblast differentiation by involving transforming growth factor-β (TGF-β) and bone morphogenetic protein (BMP) signaling [39]. Interestingly, mutations in the TGF-β1 gene are associated with Camurati-Engelmann disease (CED), which is an autosomal dominant sclerosing bone dysplasia affecting the diaphysis of long bones. CED exhibits similar long bone manifestations as GDD [40]. *Opg*/*Rankl* ratio is a vital determinant of bone mass and skeletal integrity. In this study, we show that *Ano5*$^{-/-}$ mCOBs have an elevated *Opg*/*Rankl* ratio at an early differentiation stage. At later stages, the significant difference in *Opg*/*Rankl* ratio between wt and mutant mCOBs disappears. This finding could be due to an inhibitory effect on differentiation but not on osteogenic regulation at late stages. Similarly, we found highly expressed *Opn*, which acts as a mineralization inhibitor regulating hydroxyapatite crystal growth [41] in *Ano5*$^{-/-}$ mCOBs. In order to investigate compensatory roles of other anoctamins, we investigated the expression of anoctamin 6 (*Ano6*), the closest paralog of *Ano5*. *Ano6* has been reported to up-regulate bone mineralization by activating a calcium transporter NCX1 [17, 28] or acting downstream of Runx2 and osterix. In this study, we found reduced *Ano6* expression in differentiating osteoblasts for both wild type and *Ano5*$^{-/-}$ mCOBs indicating a possible interaction with the *Ano5* gene product in calcium channel function and in matrix mineralization. Loss of *Ano6* leads to skeletal deformities and mineralization defects and results in regions of uncalcified osteoid in newborn mice with delayed mineralization [17]. Interestingly, *Ano6* expression decreased remarkably in *Ano5*$^{-/-}$ mCOB, accompanied by decreased osteoblast differentiation, and we suspect that this down-regulation of *Ano6* transcripts may compensate for the hypermineralization caused by ablation of *Ano5* in mice. Therefore, we hypothesize that *Ano5* defects lead to GDD due to reduced osteoblast differentiation and deposition of abnormal bone together with increased bone remodeling activity.

Recently, four other laboratories have reported on *Ano5* knockout mice/rabbit models. In two models with disruption of exon 1 or exon 2 of the *Ano5* gene [24, 25] investigators concluded that the defect of *Ano5*, being a phospholipid scramblase, may alter lipid metabolism and inflammation signaling or affect sperm motility. The other two knockout animals were generated by deletion of exon 8 and 9 or ablating exon 12 and/or 13. These models display defective muscle membrane fusion and repair, which may be associated with two muscular disorders, LGMD2 and MMD3 [23, 26]. Our mice were generated with a deletion of exon 11 and exon 12, which causes a frameshift in a region where at least four GDD-related mutations are located. Therefore, we believe this region is important for the pathology of the disease. Although we find no transcripts corresponding to exons downstream of exon 12 in calvariae, we do find evidence of some expressed transcripts corresponding to the 5′ region of the mRNA by qPCR. However, there is some mRNA expression downstream of exon 12 detectable in muscle. We do not know whether any protein is translated from these transcripts, but this observation raised the possibility that partial transcripts may be produced in knockout animals, which may directly or indirectly have pathogenic consequences via instable or quickly degraded proteins. In addition, we found that our 16-week-old *Ano5*$^{-/-}$ mice began to show abnormal histology in skeletal muscle (Fig. S1a) and showed decreased expression of myopathy-related factors (Fig. S1b). *Ano5*$^{-/-}$ mice also had increased serum creatine kinase (CK) levels (Fig. S1c), similar to patients with limb girdle muscular dystrophy type 2L (LGMD2L) [20].

In summary, we successfully created a mouse model for the skeletal phenotype of GDD, which recapitulates principal features of the disorder, which is the beginning of further studies to elucidate the GDD pathogenesis on a cellular and molecular level. Our results suggest that the GDD phenotype closely relates to osteoblastogenesis and bone deposition. Further studies in a knockin mouse model carrying an *Ano5* mutation for GDD will be used to study potential roles of *Ano5* mutations in GDD and will supplement studies in this knockout model.

Acknowledgements This work was supported by the National Natural Science Foundation of China (Grant # 81570958); Beijing Natural Science Foundation (Grant #7162075); High-level Talents of Beijing Health System (Grant #2013-3-036); and Scientific Foundation for the Returned Overseas Chinese Scholars, State Education Ministry (Grant # 2015-1098).

Compliance with Ethical Standards

Conflict of interest Xiaoyu Wang, Xiu Liu, Rui Dong, Chao Liang, Ernst J. Reichenberger and Ying Hu declare that they have no conflict of interest.

Human and Animal Rights and Informed Consent The animal experimentation protocols were approved by the Institutional Animal Care and Use Committee of the Beijing Stomatological Hospital (the approval number: KQYY-201611-001) and were strictly undertaken in accordance with the ethical guidelines of the Caring for Laboratory Animals by the Ministry of Science and Technology of the People's Republic of China.

References

1. Akasaka Y, Nakajima T, Koyama K et al (1969) Familial cases of a new systemic bone disease, hereditary gnathodiaphyseal sclerosis. Nippon Seikeigeka Gakkai Zasshi 43:381–394
2. Riminucci M, Collins MA, Boyde A et al (2001) Gnathodiaphyseal dysplasia: a syndrome of fibro-osseous lesions of jawbones, bone fragility, and long bone bowing. J Bone Miner Res 16:1710–1718
3. Ahluwalia J, Ly JQ, Norman E et al (2001) Gnathodiaphyseal dysplasia. Clin Imaging 31:67–69
4. Tsutsumi S, Kamata N, Maruoka Y et al (2003) Autosomal dominant gnathodiaphyseal dysplasia maps to chromosome 11p14.3–15.1. J Bone Miner Res 18:413–418
5. Jin L, Liu Y, Sun F et al (2017) Three novel ANO5 missense mutations in Caucasian and Chinese families and sporadic cases with gnathodiaphyseal dysplasia. Sci Rep 7:40935
6. Tsutsumi S, Kamata N, Vokes TJ et al (2004) The novel gene encoding a putative transmembrane protein is mutated in gnathodiaphyseal dysplasia (GDD). Am J Hum Genet 74:1255–1261
7. Marconi C, Brunamonti Binello P, Badiali G et al (2013) A novel missense mutation in ANO5/TMEM16E is causative for gnathodiaphyseal dysplasia in a large Italian pedigree. Eur J Hum Genet 21:613–619
8. Rolvien T, Koehne T, Kornak U et al (2017) A novel ANO5 mutation causing gnathodiaphyseal dysplasia with high bone turnover osteosclerosis. J Bone Miner Res 32:277–284
9. Vengoechea J, Carpenter L (2015) Gnathodiaphyseal dysplasia presenting as polyostotic fbrous dysplasia. Am J Med Genet A 167:1421–1422
10. Andreeva TV, Tyazhelova TV, Rykalina VN et al (2016) Whole exome sequencing links dental tumor to an autosomal-dominant mutation in ANO5 gene associated with gnathodiaphyseal dysplasia and muscle dystrophies. Sci Rep 6:26440
11. Duong HA, Le KT, Soulema AL et al (2016) Gnathodiaphyseal dysplasia: report of a family with a novel mutation of the ANO5 gene. Oral Surg Oral Med Oral Pathol Oral Radiol 121:123–128
12. Hartzell HC, Yu K, Xiao Q et al (2009) Anoctamin/TMEM16 family members are Ca^{2+}-activated Cl^- channels. J Physiol 587:2127–2139
13. Tran TT, Tobiume K, Hirono C et al (2014) TMEM16E (GDD1) exhibits protein instability and distinct characteristics in chloride channel/pore forming ability. J Cell Physiol 229:181–190
14. Duran C, Qu Z, Osunkoya AO et al (2012) ANOs 3–7 in the anoctamin/Tmem16 Cl^- channel family are intracellular proteins. Am J Physiol Cell Physiol 302:C482–C493
15. Di Zanni E, Gradogna A, Scholz-Starke J et al (2018) Gain of function of TMEM16E/ANO5 scrambling activity caused by a mutation associated with gnathodiaphyseal dysplasia. Cell Mol Life Sci 75:1657–1670
16. Mizuta K, Tsutsumi S, Inoue H et al (2007) Molecular characterization of GDD1/TMEM16E, the gene product responsible for autosomal dominant gnathodiaphyseal dysplasia. Biochem Biophys Res Commun 357:126–132

17. Ehlen HW, Chinenkova M, Moser M et al (2013) Inactivation of anoctamin-6/Tmem16f, a regulator of phosphatidylserine scrambling in osteoblasts, leads to decreased mineral deposition in skeletal tissues. J Bone Miner Res 28:246–259
18. Ousingsawat J, Wanitchakool P, Schreiber R et al (2015) Anoctamin-6 controls bone mineralization by activating the calcium transporter NCX1. J Biol Chem 290:6270–6280
19. Zhao P, Torcaso A, Mariano A et al (2014) Anoctamin 6 regulates C2C12 myoblast proliferation. PLoS ONE 9:e92749
20. Hicks D, Sarkozy A, Muelas N et al (2011) A founder mutation in Anoctamin 5 is a major cause of limb-girdle muscular dystrophy. Brain 134:171–182
21. Little AA, McKeever PE, Gruis KL (2013) Novel mutations in the Anoctamin 5 gene (ANO5) associated with limb-girdle muscular dystrophy 2L. Muscle Nerve 47:287–291
22. Magri F, Del Bo R, D'Angelo MG et al (2012) Frequency and characterisation of anoctamin 5 mutations in a cohort of Italian limb-girdle muscular dystrophy patients. Neuromuscul Disord 22:934–943
23. Griffin DA, Johnson RW, Whitlock JM et al (2016) Defective membrane fusion and repair in Anoctamin5-deficient muscular dystrophy. Hum Mol Genet 25:1900–1911
24. Xu J, El Refaey M, Xu L et al (2015) Genetic disruption of Ano5 in mice does not recapitulate human ANO5-deficient musculardystrophy. Skelet Muscle 5:43
25. Gyobu S, Miyata H, Ikawa M et al (2015) A role of TMEM16E carrying a scrambling domain in sperm motility. Mol Cell Biol 36:645–659
26. Sui T, Xu L, Lau YS et al (2018) Development of muscular dystrophy in a CRISPR-engineered mutant rabbit model with frame-disrupting ANO5 mutations. Cell Death Dis 9:609
27. Otaify GA, Whyte MP, Gottesman GS et al (2018) Gnathodiaphyseal dysplasia: Severe atypical presentation with novel heterozygous mutation of the anoctamin gene (ANO5). Bone 107:167–171
28. Schessl J, Kress W, Schoser B (2012) Novel ANO5 mutations causing hyper-CK-emia, limb girdle muscular weakness and Miyoshi type of muscular dystrophy. Muscle Nerve 45:740–742
29. Bolduc V, Marlow G, Boycott KM et al (2010) Recessive mutations in the putative calcium-activated chloride channel Anoctamin 5 cause proximal LGMD2L and distal MMD3 muscular dystrophies. Am J Hum Genet 86:213–221
30. Witting N, Duno M, Petri H et al (2013) Anoctamin 5 muscular dystrophy in Denmark: prevalence, genotypes, phenotypes, cardiac findings, and muscle protein expression. J Neurol 260:2084–2093
31. Sarkozy A, Hicks D, Hudson J et al (2013) ANO5 gene analysis in a large cohort of patients with anoctaminopathy: confirmation of male prevalence and high occurrence of the common exon 5 gene mutation. Hum Mutat 34:1111–1118
32. Penisson-Besnier I, Saint-Andre JP, Hicks D et al (2012) Myopathy caused by anoctamin 5 mutations and necrotizing vasculitis. J Neurol 259:1988–1990
33. Liao BY, Zhang J (2008) Null mutations in human and mouse orthologs frequently result in different phenotypes. Proc Natl Acad Sci USA 105:6987–6992
34. Chipman SD, Sweet HO, McBride DJ Jr et al (1993) Defective pro alpha 2(I) collagen synthesis in a recessivemutation in mice: a model of human osteogenesis imperfecta. Proc Natl Acad Sci USA 90:1701–1705
35. Ueki Y, Lin CY, Senoo M et al (2007) Increased myeloid cell responses to M-CSF and RANKL cause bone loss and inflammation in SH3BP2 "cherubism" mice. Cell 128:71–83
36. Chen IP, Wang CJ, Strecker S (2009) Introduction of a Phe377del mutation in ANK creates a mouse model for craniometaphysealdysplasia. J Bone Miner Res 24:1206–1215
37. Mestas J, Hughes CCW (2004) Of mice and not men: differences between mouse and human immunology. J Immunol 172:2731–2738
38. Terpstra AHM (2001) Differences between humans and mice in efficacy of the body fat lowering effect of conjugated linoleic acid: role of metabolic rate. J Nutr 131:2067–2068
39. Wahbi K, Behin A, Becane HM (2013) Dilated cardiomyopathy in patients with mutations in anoctamin 5. Int J Cardiol 16876–16879
40. Campos-Xavier B, Saraiva JM, Savarirayan R et al (2001) Phenotypic variability at the TGF-beta1 locus in Camurati-Engelmann disease. Hum Genet 109:653–658
41. Sodek J, Ganss B, McKee MD (2000) Osteopontin. Crit Rev Oral Biol Med 11:279–303